



1 **Measurement report: Nocturnal subsidence behind the cold**
2 **front enhances surface particulate matter in the plain regions:**
3 **observation from the mobile multi-lidar system**

4 Yiming Wang^{1,2}, Haolin Wang^{1,2}, Yujie Qin^{1,2}, Xinqi Xu^{1,2}, Guowen He^{1,2}, Nanxi Liu^{1,2}, Shengjie
5 Miao^{1,2}, Xiao Lu^{1,2}, Haichao Wang^{1,2,*}, Shaojia Fan^{1,2,*}

6 ¹School of Atmospheric Sciences, Sun Yat-sen University, and Southern Marine Science and
7 Engineering Guangdong Laboratory (Zhuhai), Zhuhai, 519082, China

8 ²Guangdong Provincial Observation and Research Station for Climate Environment and Air Quality
9 Change in the Pearl River Estuary, Key Laboratory of Tropical Atmosphere-Ocean System (Sun Yat-sen
10 University), Ministry of Education, Zhuhai, 519082, China

11 *Correspondence to:*

12 *Haichao Wang (wanghch27@mail.sysu.edu.cn); Shaojia Fan (eesfsj@mail.sysu.edu.cn)*

13 **Abstract.** A multi-lidar system, mounted in vehicle to monitor the profiles of temperature, wind and
14 particle optical properties, was utilized to investigate the winter fine particulate matter (PM_{2.5}) pollution
15 for a vertical perspective, in four cities in China in winter 2018. We observed the enhancement of surface
16 nocturnal PM_{2.5} in two typical plain cities (Changzhou and Wangdu), which was attributed to the
17 subsidence of PM_{2.5} transported from upstream polluted areas, with the wind turning north and
18 downdrafts dominating. Combining with the observed surface PM_{2.5}, the reanalysis meteorological data,
19 and the GEOS-Chem model simulation, we revealed the Transport-Nocturnal PM_{2.5} Enhancement by
20 Subsidence (T-NPES) events occurred frequently in the two cities, with percentages of 12.2 % and
21 18.0 %, respectively during Dec. 2018 - Feb. 2019. Furthermore, the GEOS-Chem model simulation
22 further confirmed that the ubiquity of winter T-NPES events in a large scale including North China Plain
23 and Yangtze River Delta. Process analysis revealed that the subsidence was closely correlated with the
24 southeasterly movement of the high-pressure system and the passage of the cold front, resulting in the
25 increase of temperature aloft, a stronger inversion layer, and further PM_{2.5} accumulation in the
26 atmospheric boundary layer. Thus, a conceptual model of the T-NPES events was proposed to highlight
27 this surface PM_{2.5} enhancement mechanism in these plain regions. However, it was not applicable to the
28 two cities in basin region (Xi'an and Chengdu), due to the obstruction of the weather system movement
29 by the mountains surrounding the basin.



30 **1 Introduction**

31 The severe fine particulate matter (PM_{2.5}, particles with an aerodynamic diameter smaller than 2.5 μm)
32 pollution, caused by the rapid industrialization and urbanization in China (Guo et al., 2014; Huang et al.,
33 2014), has essential impacts on visibility, ecosystem, regional and global climates, and human health
34 (Yue et al., 2017; An et al., 2019; De Marco et al., 2019; Li et al., 2019b; Hao et al., 2021). To mitigate
35 the PM_{2.5} pollution, the government of China has implemented the Air Pollution Prevention and Control
36 Action Plan in 2013 by strict emission controls (Gao et al., 2020). Despite the annual average
37 concentration of PM_{2.5} has been significantly decreased (Ding et al., 2019; Li et al., 2019a; Zhang et al.,
38 2019b; Silver et al., 2020; Geng et al., 2021b), the PM_{2.5} levels in the majority of Chinese cities are still
39 above the World Health Organization target (WHO, 2021). Particularly, the issue of PM_{2.5} pollution
40 remained critical in the North China Plain (NCP) and Yangtze River Delta (YRD) in winter time (Peng
41 et al., 2021; Qin et al., 2021).

42 The formation mechanisms of PM_{2.5} pollution were complex especially in China (Guo et al., 2014; Xiao
43 et al., 2021b). Such as the high emission intensity (Zhang et al., 2019b), the rapid chemical formation of
44 secondary particles owing to the gas-phase and heterogeneous reactions (Wang et al., 2017; Lu et al.,
45 2019; Chen et al., 2020), and the interactions within the atmospheric boundary layer (ABL) (Ding et al.,
46 2013; Gao et al., 2016; Dong et al., 2017; Li et al., 2017). While the long-range transport also had
47 significant impacts on the PM_{2.5} pollution (Guo et al., 2014; Zhang et al., 2015; Huang et al., 2018). Cold
48 fronts, as a common synoptic circulation in winter, were usually favourable for the quick removal of the
49 locally accumulated pollutants in the NCP (Zhao et al., 2013; Gao et al., 2017), but conversely transport
50 the pollutants to the YRD through a long distance (Kang et al., 2019; Huang et al., 2020; Kang et al.,
51 2021). Zhou et al. (2023) indicated that the cold fronts could transport the precursors to the residual layer,
52 where the secondary pollution was rapidly driven to be generated and then exacerbate near-surface air
53 pollution as a result of the development of the daytime convective ABL. However, the above studies
54 have focused on the impact of the horizontally transported pollutants on the downstream regions after
55 the passage of the cold front. While few studies have been conducted on the variation in the vertical
56 direction of particulate matter in the ABL during the passage of the cold front.

57 The vertical mixing exchange process between layer has great impacts on local air quality and the
58 subsidence motion is associated with the evolution of inversion layer (Gramsch et al., 2014; Xu et al.,
59 2018; He et al., 2022). Zhang et al. (2022) reported that the PM_{2.5} concentration behind the cold front
60 increased due to the subsidence motion and inversion layer. Zhao et al. (2023) suggested that the frontal



61 downdrafts were an additional transport pathway in the nighttime to make higher contribution to the
62 ground nitrate. Both of their studies were based on the model simulations, the observational evidence of
63 the subsidence behind the cold front and its impact on the nocturnal PM_{2.5} enhancement events is still
64 lacking. Shi et al. (2022) reported one subsidence case of particulate matter during the passage of the
65 cold front over Wangdu, China in winter, which revealed that the subsidence was closely connect to the
66 enhancement of nocturnal PM_{2.5}.

67 To investigate the mechanisms of nocturnal PM_{2.5} enhancement triggered by subsidence, the three-
68 dimensional spatial and temporal distribution is crucial. Many field observations of the vertical
69 distribution of particulate matter have been performed employing various methods such as tethered
70 balloons (Wang et al., 2021; Ran et al., 2022), airplane (Wang et al., 2018; Fast et al., 2022), unmanned
71 aerial vehicles (Song et al., 2021; Dubey et al., 2022) and the meteorological towers (Li et al., 2022; Yin
72 et al., 2023). Lidar, as an active remote sensing device with high temporal and spatial resolution, has
73 been extensively employed in atmospheric detection to obtain the profile of particulate matter, wind, and
74 temperature. The ground-based and satellite-based lidar have been widely used to detect the vertical
75 distribution of aerosol. In recent years, the mobile multi-lidar system has been gradually developed and
76 has become a powerful tool to observe the development of target species detection in a vertical
77 perspective. Compared with the traditional ground-lidar system, the mobile multi-lidar system enables
78 continuous mobile observations and provides information on the distribution of specific factors along its
79 path and can be used as an effective supplement to other fixed lidars. Additionally, the mobile multi-
80 lidar system can reach different cities by its portable setting in a short time to carry out the fixed-point
81 observations. The mobile lidar system had been used to carry out several observations in the past few
82 years (Lv et al., 2020; He et al., 2021; Xu et al., 2022). He et al. (2021) investigated the vertical
83 distribution characteristics of particulate matter in the Guanzhong Plain by using the mobile multi-lidar
84 system. Xu et al. (2022) conducted an observational study on the three-dimensional structure of
85 particulate matter distribution in the Guangdong-Hong Kong-Macao Greater Bay Area by using the
86 mobile multi-lidar system and proposed a conceptual model to elucidate the vertical distribution of
87 particulate matter under different wind and temperature conditions.

88 Here, we conducted the first nationwide field measurements in winter 2018 using the mobile multi-lidar
89 system during winter 2018 in China, to investigate the vertical distribution characteristics of particulate
90 matter in different cities. We focus on the observed nocturnal PM_{2.5} enhancement events and seek insights
91 into their characteristics and the causes, by combining the GEOS-Chem model simulation, the surface



92 PM_{2.5} observation and meteorological reanalysis dataset. Finally, we examine the ubiquity of this
93 phenomenon in plain regions in China and propose a conceptual model, providing detailed vertical
94 insights into the enhancement of nocturnal surface PM_{2.5}.

95 **2 Data and methods**

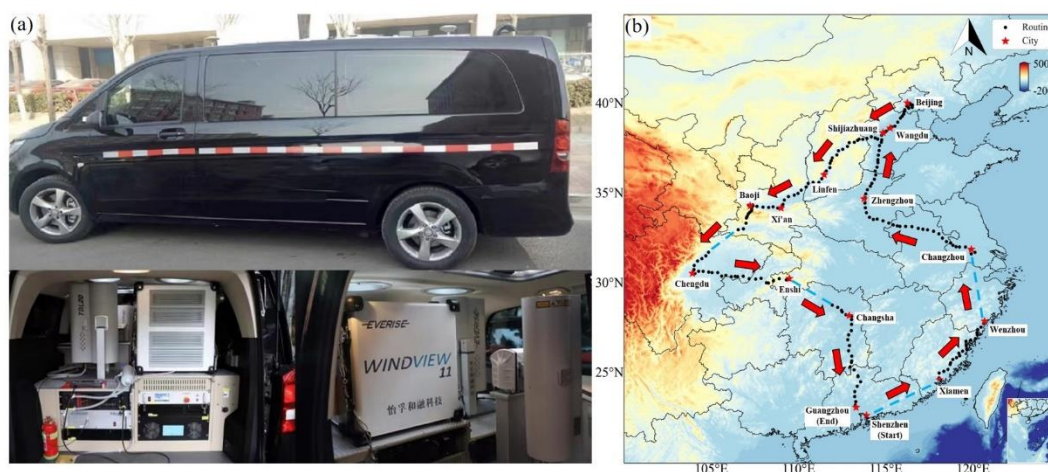
96 **2.1 Multi-lidar system**

97 A multi-lidar system was installed on the mobile observation vehicle. The vehicle, a modified 7-seater
98 Mercedes-Benz sport utility vehicle, was equipped with three lidar instruments mounted on steel bars at
99 the rear for stability. The mobile observation routes were primarily on flat highways, and the speed was
100 controlled to remain around 80 km/h to minimize the impact of frequent changes in speed and vehicle
101 bumps on the measurement results.

102 The multi-lidar system (Everise Technology Ltd., Beijing) consisted of a 3D visual scanning micro pulse
103 lidar (EV-Lidar-CAM), a twirling Raman temperature profile lidar (TRL20), a Doppler wind profile lidar
104 (WINDVIEW10), a global positioning system (GPS). The 3D visual scanning micro pulse lidar had a
105 detection range of up to 30 km, a temporal resolution of 1 minute, and a vertical resolution of 15 m. The
106 3D lidar emitted a 532 nm laser beam vertically, which is scattered by aerosol particles in the atmosphere.
107 The backscattered signal is utilized to calculate the aerosol extinction coefficient and depolarization ratio
108 profile. The extinction coefficient increases with higher particle pollution concentrations, while the
109 depolarization ratio can distinguish between spherical and non-spherical particles based on their size and
110 shape. The Doppler wind profile lidar provides a temporal resolution of 1 minute and a vertical resolution
111 of 50 m. It emits a rotating 1545 nm laser beam and measures the Doppler shift produced by the laser's
112 backscattered signal as it passes through airborne particles such as dust, water droplets in clouds and fog,
113 polluted aerosols, salt crystals, and biomass-burning aerosols to derive the horizontal and vertical wind
114 speeds at any height. The Raman temperature profile lidar, based on Raman scattering theory, calculates
115 atmospheric temperature by detecting the rotational Raman scattering signal of nitrogen or oxygen
116 molecules in the atmosphere. Operating at a 532 nm wavelength, it has a temporal resolution of 5 minutes
117 and a vertical resolution of 60 m. The quality of the data obtained by the lidar system was checked by
118 the Integrated Environmental Meteorological Observation Vehicle before deployment. The results
119 showed a percentage difference of less than 15% between the lidar system data and the data provided by
120 the Shenzhen Meteorological Tower, demonstrating the high accuracy of the lidar instrument (Xu et al.,



121 2022). Previous studies had utilized this lidar system and demonstrated its reliability (Xu et al., 2018; He
122 et al., 2021). The mobile observation vehicle and multi-lidar system are shown in Figure 1(a).



123

124 **Figure 1.** (a) The mobile observation vehicle and multi-lidar system. (b) The mobile observation route and stopover
125 cities, the blue dotted line shows the sections of missing data.

126 2.2 The route of nationwide mobile observation

127 To investigate the distribution characteristics of particulate matter during winter in different regions in
128 China, the Integrated Environmental Meteorological Observation Vehicle of Sun Yat-sen University was
129 utilized to conduct the first nationwide mobile observation campaign. The campaign, which lasted 43
130 days and covered approximately 11,000 km, started in Shenzhen on 30 November, 2018 and ended in
131 Guangzhou on 11 January, 2019. This campaign surveyed the $PM_{2.5}$ vertical profiles across 15 cities,
132 including Shenzhen, Xiamen, Wenzhou, Changzhou, Zhengzhou, Wangdu, Beijing, Shijiazhuang,
133 Linfen, Xi'an, Baoji, Chengdu, Enshi, Changsha and Guangzhou. The observation route and stopover
134 cities are shown in Figure 1(b). Due to the precipitation, there were no observations between Shenzhen-
135 Xiamen and Wenzhou-Changzhou, while some GPS data were missing between Beijing-Chengdu and
136 Enshi-Changsha.

137 To compare the vertical distribution characteristics of particulate matter in different regions, we
138 conducted fixed-point observations for several pollution days in four representative cities in the East
139 China region (Changzhou), North China Plain (Wangdu), Guanzhong Basin (Xi'an), and Sichuan Basin
140 (Chengdu). The dates and duration of the fixed-point observations are presented in Table 1. In the



141 following analysis, only the data obtained in the four fixed-point measurements are used since it has an
142 enough time duration to show the vertical variation of PM_{2.5}.

143 **Table 1.** Date and cities of fixed-point observations

Date	Cities	Coordinate	Landform
2018.12.11-2018.12.14	Changzhou	119.97°E, 31.83°N	Plain area
2018.12.18-2018.12.22	Wangdu	115.25°E, 38.67°N	Plain area
2018.12.31-2019.01.02	Xi'an	109.01°E, 34.22°N	Basin area
2019.01.04-2019.01.09	Chengdu	103.92°E, 30.58°N	Basin area

144

145 **2.3 Surface PM_{2.5} data and ERA5 reanalysis data**

146 The nationwide hourly observations of surface PM_{2.5} in China are obtained from the China National
147 Environmental Monitoring Center (CNEMC) network (<https://quotsoft.net/air>, last accessed: March 2nd,
148 2023). Here, we used the hourly PM_{2.5} concentration data from the whole winter of 2018 (Dec. 2018 –
149 Feb. 2019) and selected data from the closest monitoring station to show the change in surface PM_{2.5}
150 concentration at the four observation sites.

151 The spatial distribution of daily average surface PM_{2.5} concentration is obtained from the TAP team
152 (<http://tapdata.org.cn>), with spatial resolution of 10 km. Based on machine learning algorithms and multi-
153 source data information, the TAP team has built a multi-source data fusion system that integrates ground
154 observation data, satellite remote sensing information, high-resolution emission inventories, air quality
155 model simulations and other multi-source information (Geng et al., 2021a; Xiao et al., 2021a). In addition
156 to the observation data, we also apply the three-dimensional meteorological data from ERA5 dataset for
157 the winter of 2018 (<https://quotsoft.net/air>, last accessed: March 2nd, 2023) (Munoz-Sabater et al., 2021).
158 This dataset contained temperature, horizontal and vertical wind speed, and direction at pressure levels,
159 as well as two-dimensional data including sea-level pressure and 2-m temperature. The ERA5 dataset is
160 the fifth generation of the European Centre for Medium-Range Weather Forecasts (ECMWF)
161 atmospheric reanalysis of the global climate. The ERA5 dataset has a horizontal resolution of
162 0.25°×0.25°, a vertical resolution of 25 hPa, and a temporal resolution of 1 h.



163 **2.4 HYSPLIT backward trajectory model**

164 The Hybrid Single Particle Lagrangian Integrated Trajectory Model (HYSPLIT) (Stein et al., 2015),
165 developed by NOAA Air Resources Laboratory, which is a valuable tool for simulating the movement
166 of air mass and the transport of pollutants in the atmosphere, is used in our study to obtain the sources of
167 particulate matter at different heights. Altitudes of 100, 500, and 1000 m were set as the end points of
168 the trajectories, the meteorological input for the trajectory model was the FNL dataset, and each trajectory
169 was calculated for 24 h duration.

170 **2.5 GEOS-Chem model description**

171 Given the short-term (less than one week) fixed-point observation duration of the mobile observation
172 vehicle in each city, we employ the global three-dimensional chemical transport model GEOS-Chem
173 version 13.3.1 to interpret the vertical observations (available at
174 <https://github.com/geoschem/GCClassic/tree/13.3.1>, last assessed: March 2nd, 2023, (Bey et al., 2001))
175 and to simulate the distribution of particulate matter concentrations during winter 2018 in China. We
176 perform the nested-grid version of GEOS-Chem simulation at a spatial of 0.5° (latitude) \times 0.625°
177 (longitude) resolution over East Asia ($60\text{--}150^\circ\text{E}$, $11^\circ\text{S}\text{--}55^\circ\text{N}$). The model has 47 vertical layers with 18
178 layers in the below 3 km. Boundary chemical conditions for the nested models are archived from a
179 consistent global simulation run at 4° latitude \times 5° longitude resolution. Meteorological input is from the
180 Modern-Era Retrospective analysis for Research and Application version 2 (MERRA-2) (Gelaro et al.,
181 2017). We conduct the model simulation from 2018/11-2019/02 with the first one month as spin-up.
182 The model mechanisms and emissions mostly follow our previous study (Wang et al., 2022). In short,
183 the GEOS-Chem model describes a comprehensive stratospheric and tropospheric ozone–NO_x–VOCs–
184 aerosol–halogen chemical mechanism (Wang et al., 1998; Park et al., 2004; Parrella et al., 2012; Mao et
185 al., 2013). Photolysis rates are computed using the Fast-JX scheme (Bian and Prather. 2002). Advection
186 of tracers in GEOS-Chem is accomplished through TPCORE advection algorithm. Boundary layer
187 mixing process is described in (Lin and McElroy. 2010). Dry and wet deposition of both gas and aerosols
188 is considered (Wesely. 1989; Zhang et al., 2001). We apply the latest version of the Community
189 Emissions Data System (CEDSV2) anthropogenic emissions inventory (O'Rourke et al., 2021), in which
190 the emissions over China have been adjusted to align with the Multi-resolution Emission Inventory for
191 China (MEIC) inventory (Zheng et al., 2018).



192 **3 Results and discussions**

193 **3.1 The observation of nocturnal PM_{2.5} enhancement in plain areas**

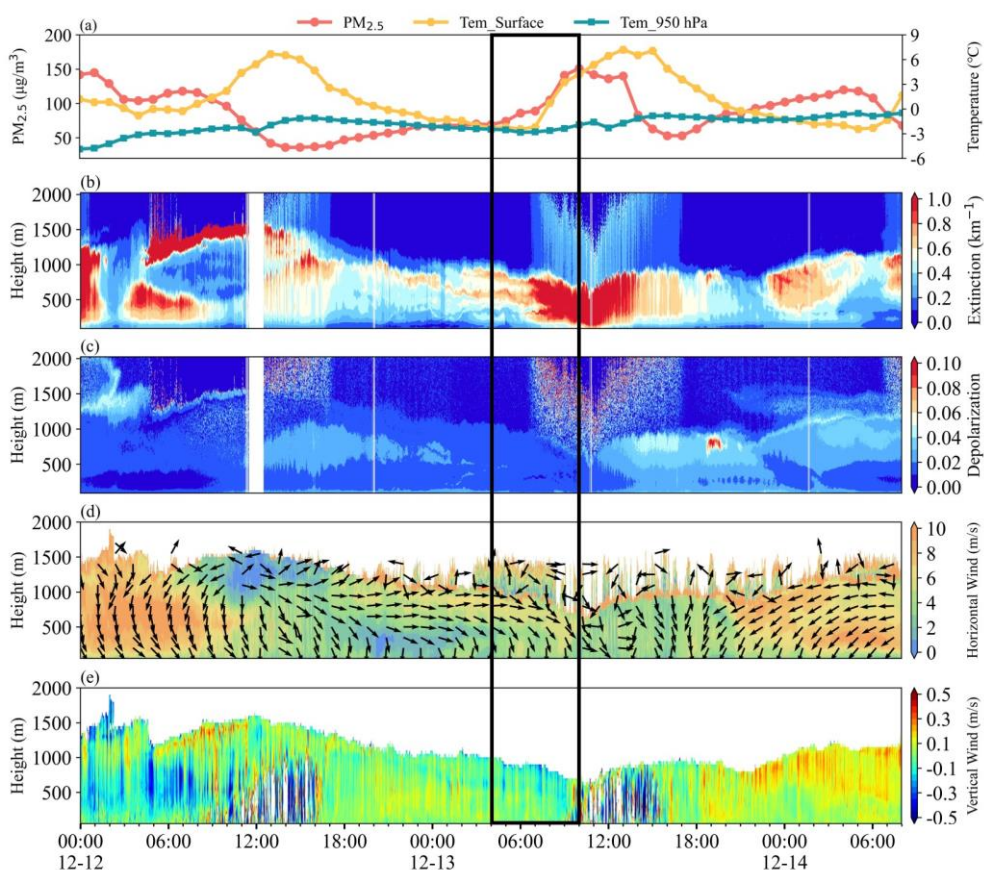
194 During the fixed-point observation in Changzhou, we observed a typical surface PM_{2.5} concentration
195 enhancement event starting at 4:00 and lasting until 10:00 on 13 December. As shown in Figure 2(a), the
196 concentration of PM_{2.5} increased from 69 to 151 $\mu\text{g}/\text{m}^3$. Figure 2(b-c) showed the spatiotemporal
197 distribution of the extinction coefficient and depolarization ratio. There was a clear layer with low
198 extinction coefficient below 500 m from 16:00 on 12 December to 4:00 on 13 December, indicating low
199 PM_{2.5} concentration near the surface. Meanwhile, an aerosol layer with high extinction coefficient of
200 about 0.7 km^{-1} appeared at 500-1,000 m. Figure 2(d-e) depicted the west winds prevailed the layer of
201 500-1,000 m with a wind speed (WS) of about 7 m/s. Based on the daily averaged concentration of PM_{2.5}
202 on 12 December shown in Figure S1, the west area of the observation site in Changzhou suffered from
203 severe air pollution with the concentration of PM_{2.5} exceeding $150 \mu\text{g}/\text{m}^3$. Under the strong forcing of
204 the west winds, the regional transport of aerosol from the west of Changzhou was detected, leading to a
205 high extinction coefficient layer at 500-1,000 m. The spatiotemporal distribution of the vertical velocity
206 in Figure 2(e) indicated the dominant updraft winds in the ABL, which was conducive to the suspension
207 of pollutants at 500-1,000 m.

208 However, the prevailing winds at 500-1,000 m shifted to the northwest/north after 4:00 on 13 December.
209 By 8:00, the north wind dominated in the ABL. The change in wind direction affected the transport
210 process of pollutants at 500-1,000 m, after which the transport basically disappeared. Meanwhile, the
211 downdraft winds dominated above 500 m (Figure 2(e)) and the aerosol layer suspended at the 500-1,000
212 m began to gradually transport and diffuse downward into the lower layer of ABL, which enhanced the
213 nocturnal surface PM_{2.5} concentration. Noteworthy, after 4:00 on 13 December, the surface temperature
214 was close to the temperature at 950 hPa, suggesting that the structure of the ABL was stable and was
215 conducive to the accumulation of the PM_{2.5}.

216 The sea surface field showed the cold high-pressure system moved southeast with increasing strength
217 from 20:00, 12 December to 8:00, 13 December (Figure S2). The change in the synoptic weather system
218 was accompanied by a cold frontal passage. The cold frontal passage was inferred to start at about 4:00,
219 13 December and last about 4 hours, which was further illustrated by the clockwise rotation of the
220 horizontal wind from ground to upper layer (Shi et al., 2022) and the transition from updrafts to
221 downdrafts, the observation site was located behind the cold front after 4:00 where the descending



222 movements dominated. Under the influence of the subsidence, the pollutants transported by the west
 223 advection diffused downward to the low layer and further aggravated the local air quality.



224

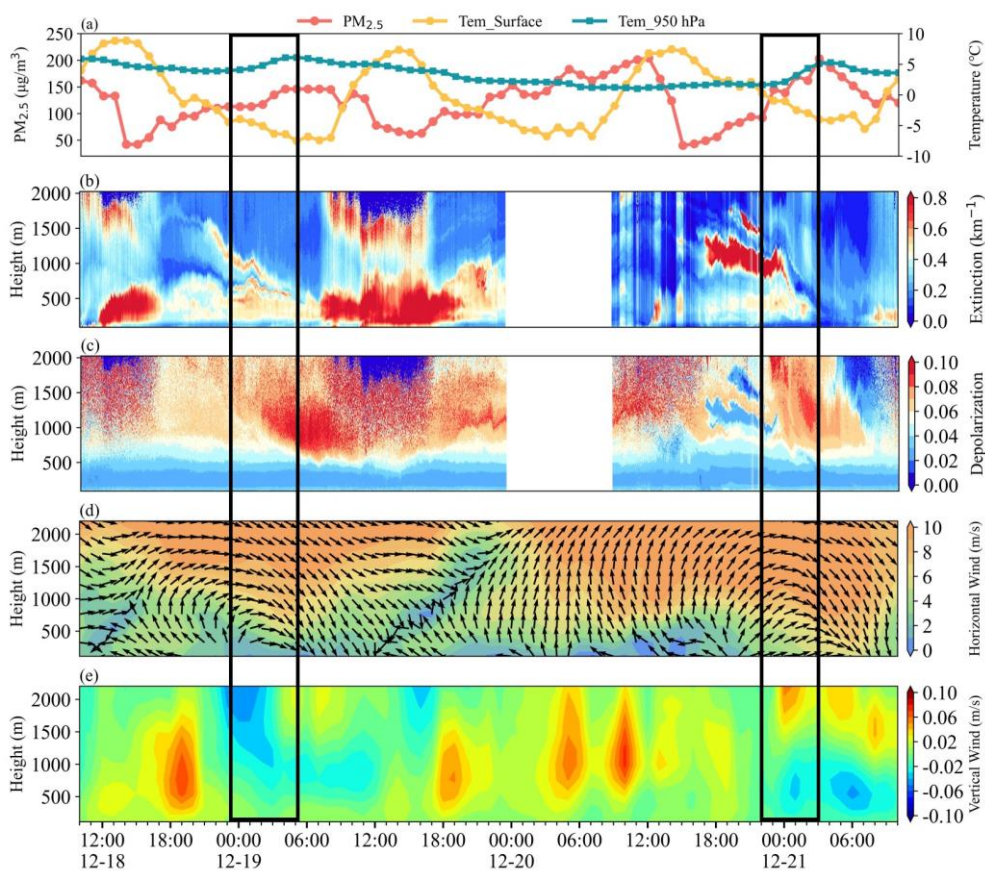
225 **Figure 2.** (a) Surface PM_{2.5} concentration, surface temperature and 950 hPa temperature, (b) Extinction coefficient,
 226 (c) Depolarization ratio, (d) Horizontal wind, and (e) Vertical wind, during the observation in Changzhou from 12
 227 December to 14 December. The black box indicated the nocturnal surface PM_{2.5} enhanced event.

228 After 8:00, the concentration of surface PM_{2.5} increased rapidly and peaked at around 10:00, the
 229 extinction coefficient below 1,000 m also reached a high level with 1.0 km⁻¹ at the same time and the
 230 depolarization remained about 0.01. The surface temperature began to rise and the convective ABL
 231 developed rapidly, which enhanced the vertical mixing and resulted in the rapid increase in surface PM_{2.5}
 232 (Zhou et al., 2023). And the north winds following the passage of the cold front dominated in the ABL
 233 after 8:00, which could bring pollution from the NCP to the YRD (Kang et al., 2019; Huang et al., 2020).



234 Therefore, we attribute the increase in the concentration of surface $PM_{2.5}$ from 4:00 to 10:00 to the
235 combination of the subsidence behind the cold front before 8:00, vertical mixing caused by the
236 development of the convective ABL, and the transport by the north winds.

237 We also found similar nocturnal surface $PM_{2.5}$ enhancement events during the fixed-point observation in
238 Wangdu, on 19 December and 21 December respectively (Figure 3(a)). The concentration of $PM_{2.5}$
239 started to enhance at 1:00, 19 December, and meanwhile, the layer of pollutants above 1,000 m started
240 to transport and diffuse to the lower layer of ABL which was reflected by the change of the extinction
241 coefficient shown in Figure 3(b). Unfortunately, due to the instrument malfunction, the wind profile data
242 was unavailable and we used the ERA5 data instead, which previously showed good consistent with the
243 observation of with Doppler wind lidar (Shi et al., 2022). As shown in Figure 3(d), from 10:00, 18
244 December to 0:00, 19 December, southwest winds prevailed above 1,000 m and the WS exceeded 8 m/s,
245 a persistent southerly wind could result in severe air pollution in the NCP (Cai et al., 2017; Callahan et
246 al., 2019; Zhang et al., 2019a). The wind forced the regional advection of pollutants from the south region
247 suffered from serious air pollution (Figure S3) to the observation site. Meanwhile, the updrafts dominated
248 in the ABL which facilitated the suspension of pollutants in the upper layer. After 0:00, 19 December,
249 as the cold high-pressure system moved southwest accompanied by a cold front (Figure S4), the
250 prevailing winds above 1,000 m shifted to northwest gradually and downdrafts dominated behind the
251 cold frontal passage. The changes in the horizontal and vertical wind fields caused the advection of
252 pollutants to disappear basically and the pollutants layer suspended above 1,000 m began to transport
253 and diffuse downward to the low layer of ABL. The passage of the cold front at 0:00, 19 December,
254 lasted for 4 hours, and the subsidence behind the cold front caused the pollutants to diffuse downward,
255 enhancing the concentration of nocturnal $PM_{2.5}$.



256

257 **Figure 3.** (a) Surface PM_{2.5} concentration, surface temperature and 950 hPa temperature, (b) Extinction coefficient,
 258 (c) Depolarization ratio, (d) Horizontal wind, and (e) Vertical wind, during the observation in Wangdu from 18
 259 December to 21 December. The black boxes indicated the Nocturnal PM_{2.5} enhancement events.

260 The pattern of the nocturnal surface PM_{2.5} enhancement event on 21 December was highly similar to that
 261 on 19 December. However, the pollutant advection process lasted a longer duration which started at
 262 16:00, 20 December and ended at 0:00, 21 December (Figure 3(b)), and the WS of the southwest wind
 263 above 1,000 m exceeded 12 m/s meeting the standard of the low-level jet (LLJ) (Kraus et al., 1985; Hu
 264 et al., 2013). The area south of the observation site in Wangdu suffered from more severe air pollution
 265 with the concentration of PM_{2.5} exceeding 300 μg/m³ (Figure S5). Under the strong forcing of the
 266 southwester LLJ and the updrafts depicted in Figure 3(d-e), an aerosol layer with high extinction
 267 coefficient exceeding 2 km⁻¹ formed and was suspended at 1,000-1,500 m from 16:00, 20 December to



268 0:00, 21 December. Meanwhile, Figure 3(c) showed that the layer with low depolarization was consistent
269 with the layer with high extinction coefficient, further confirmed the role of transportation.

270 After 0:00, the wind direction of LLJ began to change due to the southeasterly movement of the high-
271 pressure system accompanied a cold front (Figure S6). The passage of cold front started at 0:00, 21
272 December and lasted for 4 hours, after which the downdrafts dominated below 1,500 m (Figure 3(e)),
273 and the northwester LLJ no longer transported pollutants from the southern area but greatly enhanced
274 the turbulent mixing (Shi et al., 2022). Under the influence of the turbulence generated by LLJ and
275 subsidence behind the cold front, the aerosol-rich layer suspended at 1,000-1,500 m was gradually
276 transported and diffused downward into the lower layer of ABL, ultimately enhancing the concentration
277 of surface $PM_{2.5}$, which was consistent with the result reported by (Shi et al., 2022), with the secondary
278 inorganic aerosol increasing simultaneously during the subsidence process as observed by the tethered
279 balloon.

280 Noteworthy, when both nocturnal surface $PM_{2.5}$ enhancement events in Wangdu occurred, the
281 temperature at 950 hPa showed an increasing trend as a result of the heating of the air by compression as
282 it descended, while the surface temperature continuously declined (Figure 3(a)). The opposite variation
283 of surface temperature and temperature at 950 hPa stabilized the lower atmosphere. The stronger
284 inversion layer was probably induced by subsidence (Carlson and Stull. 1986). With the more stably
285 atmospheric layer and inversion during subsidence, the concentration of surface $PM_{2.5}$ enhanced
286 (Gramsch et al., 2014; LARGERON and Staquet. 2016).

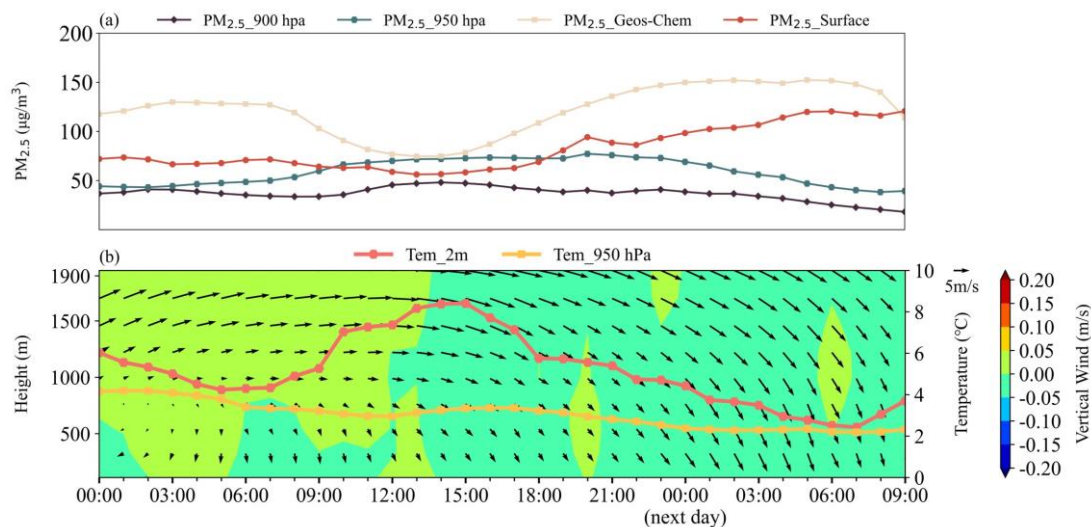
287 **3.2 Transport-Nocturnal $PM_{2.5}$ Enhancement by Subsidence events**

288 During the fixed-point observation, we found the causes of three nocturnal $PM_{2.5}$ enhancement events in
289 different cities were similar. The processes included three steps: First, the horizontal winds with high
290 wind speed forced the transport of pollutants from the upstream region, while the updrafts dominated,
291 both resulting in the formation and suspension of an aerosol layer with high extinction coefficient at the
292 high layer of the ABL. Then, under the influence of the southeasterly movement of high-pressure system
293 and the passage of the cold front, the horizontal wind direction shifted to north or northwest and the
294 downdrafts became dominant. Finally, the transport of pollutants disappeared due to the change of wind
295 direction, and under the subsidence behind the cold front, the aerosol-rich layer suspended at high layer
296 was gradually transported and diffused downward into the lower layer of the ABL, ultimately enhancing



297 the concentration of nocturnal $PM_{2.5}$. Here, we defined this pollution pattern as T-NPES (Transport-
298 Nocturnal $PM_{2.5}$ Enhancement by Subsidence) events.

299 To investigate the occurrence frequency of T-NPES events, we employed the GEOS-Chem model to
300 simulate the distribution of particulate matter concentrations in China during the whole winter of 2018
301 (Dec. 2018 – Feb. 2019). We utilized the simulated $PM_{2.5}$ at 950 hPa and 900 hPa to represent the high-
302 altitude $PM_{2.5}$ concentration. We selected the closest grid data of the wind field data, 950 hPa and 2-m
303 temperature data from ERA5 dataset to the observation site in Changzhou and Wangdu to show the
304 meteorological condition. By analysing the hourly concentration variation of $PM_{2.5}$ and the distribution
305 of the wind field during the three months of winter 2018 in Changzhou and Wangdu, we found 11 typical
306 T-NPES events in Changzhou accounting for 12.2% and 18 T-NPES events in Wangdu accounting for
307 18%, which indicated that the T-NPES events were a relatively common phenomenon in the two cities.
308 Figure 4 showed the average pattern of all T-NPES events in Changzhou, the trend of the simulated $PM_{2.5}$
309 was consistent with the observation, confirming the credibility of the simulations. As shown in Figure
310 4(a), the enhancement of nocturnal surface $PM_{2.5}$ started at 21:00, when there was no significant
311 enhancement in anthropogenic $PM_{2.5}$ emissions, while the high-altitude $PM_{2.5}$ represented by $PM_{2.5}$ at
312 900 hPa and 950 hPa started to decrease, which was consistent with the observed event in Changzhou
313 described in Section 3.1. According to the distribution of wind field (Figure 4(b)), west winds with high
314 wind speed prevailed the layer above 1,000 m from 0:00 to about 18:00, which was conducive to the
315 transport of pollutants. And the updrafts dominated from 0:00 to 12:00, forcing the pollutants suspending
316 in the upper layer, which was reflected by the enhancing $PM_{2.5}$ concentration at high-altitude (Figure
317 4(a)). Despite the downdrafts dominated after 12:00, there was no immediate reduction in $PM_{2.5}$
318 concentration at high-altitude, which might be related to the fact that the horizontal wind direction had
319 not changed, and the transport of pollutants continued. A brief updraft before 21:00 suspended the
320 pollutants at high-altitude. After 21:00, northwester winds and downdrafts dominated in the ABL and
321 the high-altitude $PM_{2.5}$ began to gradually transport and diffuse downward causing the enhancement of
322 surface concentration of $PM_{2.5}$, and this process continued until 4:00 in the next day. The surface
323 temperature and the temperature at 950 hPa gradually approached, which is consistent with the observed
324 case in Changzhou, indicating that the structure of the ABL was stable and was conducive to the
325 accumulation of the $PM_{2.5}$. As shown in Figure S7, the average sea level pressure indicated that the
326 southeasterly movement of the high-pressure system and the passage of cold front, which resulted in the
327 shift in wind direction and subsidence behind the cold front, were the main causes of the T-NPES events.



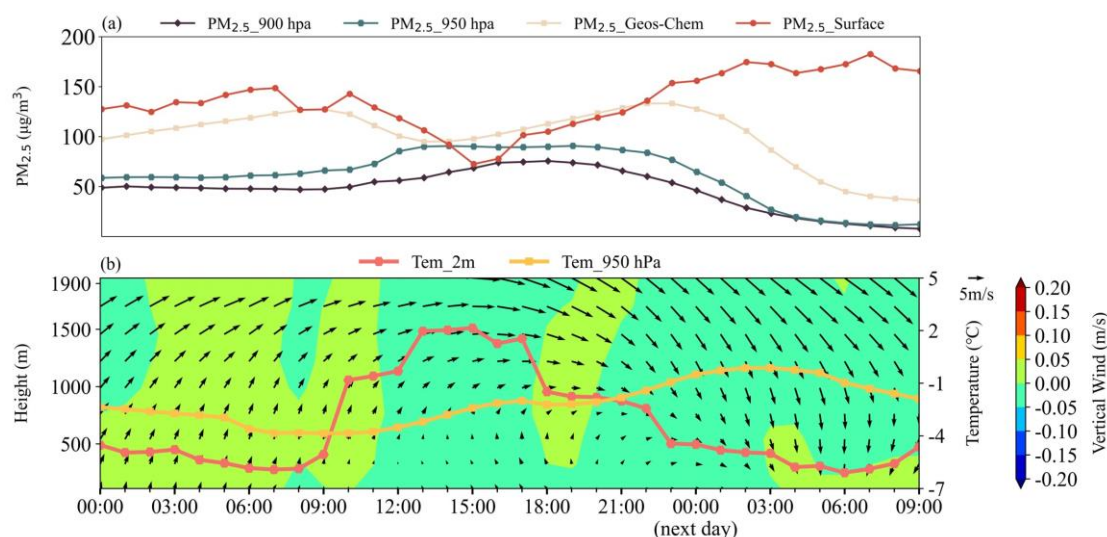
328

329 **Figure 4.** The average for all T-NPES events in Changzhou. (a) The concentration of PM_{2.5} at different levels,
 330 surface PM_{2.5} of observation (red line), surface PM_{2.5} of simulation (blue line), PM_{2.5} at 900 hPa and 950 hPa. (b)
 331 The horizontal winds (arrows), the vertical winds (shaded), temperature at 2 m and temperature at 950 hPa.

332 Figure 5 showed the average pattern of all T-NPES events in Wangdu, which was similar to that in
 333 Changzhou. Figure 5(a) demonstrated that the trend of simulated PM_{2.5} was consistent with the
 334 observation before 22:00 but was different thereafter. The trend of high-altitude PM_{2.5} was increasing
 335 before 15:00 due to the transport of pollutants by prevailing southwester horizontal winds and the
 336 dominant of updrafts which suspended the aerosol shown in the Figure 5(b). After 18:00, the prevailing
 337 winds began to turn to northwest and ultimately turn to north at 0:00 in the next day, while a brief updraft
 338 between 18:00 and 20:00 suspended the pollutants at high-altitude. The ABL was dominated by the
 339 northwester winds and downdrafts after 21:00. Simultaneously, the high-altitude PM_{2.5} began to
 340 gradually transport and diffuse downward causing the enhancement of surface concentration of PM_{2.5}.
 341 The temperature at 950 hPa increased and the surface temperature declined (Figure 5(b)), which agreed
 342 with the two observation examples in Wangdu. The opposite variation of temperature at different height
 343 stabilized the ABL and further enhanced the concentration of PM_{2.5}. By analysing the weather circulation
 344 patterns, the causes of the T-NPES events were the same with those in Changzhou and were attributed
 345 to the southeasterly movement of high-pressure system and the passage of the cold front (Figure S8).
 346 Overall, the average patterns of T-NPES events in Changzhou and Wangdu were essentially in good
 347 agreement with the three cases of T-NPES in the two cities. But there were still slight differences, such



348 as the change of Wangdu caused by the movement of high-pressure lasted a longer time in the average
 349 situation and the start time of subsidence behind the cold front was also not consistent, which were due
 350 to each T-NPES event was not exactly the same.



351
 352 **Figure 5.** The average for all T-NPES events in Wangdu. (a) The concentration of PM_{2.5} at different levels, surface
 353 PM_{2.5} of observation (red line), surface PM_{2.5} of simulation (blue line), PM_{2.5} at 900 hPa and 950 hPa. (b) The
 354 horizontal winds (arrows), the vertical winds (shaded), temperature at 2 m and temperature at 950 hPa

355 3.3 The universality of T-NPES events in eastern China

356 Despite the mobile observation vehicle had no observations in other cities of the NCP, the YRD and the
 357 Loess Plateau, we could still utilize the simulated data and the ERA5 data to investigate the universality
 358 of T-NPES events occurrence in other cities. We selected Shijiazhuang, Beijing and Tianjin as
 359 represented cities of the NCP, Shanghai and Nanjing as represented cities of the YRD and Taiyuan,
 360 Linfen as represented cities of the Loess Plateau. We found the similar pattern of T-NPES events in all
 361 these cities. However, these T-NPES events in different cities had some differences in detail. Here we
 362 divided the T-NPES events into four types based on the status of PM_{2.5} after T-NPES events. More
 363 information on the types, frequency of the T-NPES events and their percentage of the winter 2018 was
 364 shown in Table 2.

365 The typical representation of Type 1 was shown in Figure S9, the characteristic of Type 1 was that the
 366 southwester winds transported the pollutants in high-altitude of the ABL, then the wind direction shifted
 367 to north and downdrafts dominated, finally, pollutants in high-altitude diffused into lower layer causing



368 the surface $PM_{2.5}$ enhanced. However, after T-NPES event, the north wind near the ground was not strong
 369 enough to remove the pollutants, causing the high level of $PM_{2.5}$ lasting the next day morning and may
 370 resulting in aggravation of the air pollution in the following day. The characteristic of T-NPES event of
 371 Type 2 was basically consistent with Type 1. However, after the T-NPES event, as north winds became
 372 stronger, pollutants were rapidly removed, resulting in a clean boundary layer throughout (Figure S10).
 373 Even when the pollutants were removed more quickly by stronger north winds, the subsidence process
 374 might not be observed. Type 1 and Type 2 were both observed in the NCP cities, while Type 1
 375 predominated in Wangdu and Shijiazhuang, and Type 2 in Beijing and Tianjin.

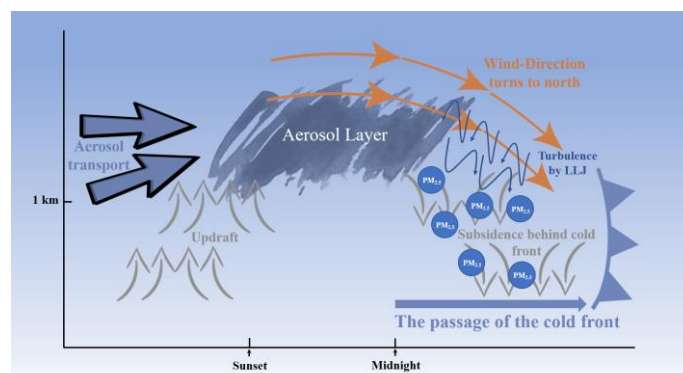
376 **Table 2.** Statistics of the T-NPES events in cities during Dec. 2018 – Feb. 2019

Area	Type	City	Frequency (days)	Percentages
NCP	Type 1 and 2	Wangdu	18	20.0%
		Shijiazhuang	18	20.0%
		Beijing	13	14.4%
		Tianjin	14	15.6%
YRD	Type 3	Changzhou	11	12.2%
		Shanghai	7	7.8%
		Nanjing	8	8.9%
Loess Plateau	Type 4	Linfen	18	20.0%
		Taiyuan	13	14.4%

377
 378 Figure S11 showed the typical representation of Type 3. The prevailing wind transporting pollutants was
 379 not southwest but west and the start and end of the T-NPES event were later than for Type 1 and 2. After
 380 the T-NPES event, the increase of 2-m temperature and the development of convective ABL led to the
 381 vertical mixing and the increase of surface $PM_{2.5}$. Additionally, the stronger north wind might transport
 382 the pollutants from the NCP to the YRD. The Type 3 was similar to the example in Changzhou in Section
 383 3.1 and indicative of a typical pattern in the YRD cities.
 384 The typical representation of Type 4, which was mainly occurred in the Loess Plateau cities, was shown
 385 in Figure S12. During the T-NPES event, the change of wind direction was only observed above 1,500
 386 m while the wind speed below was so weak that the shift in wind direction was not significant, which
 387 was significantly different from the wind field of other three types. The reason for the difference between



388 Type 4 and other types was mainly related to the topography of the Loess Plateau, which has a blocking
389 effect on the movement of high-pressure system. Noteworthy, after the analysis of these T-NPES events
390 in different cities in China, we suggested that the T-NPES events were a common pattern of the nocturnal
391 $PM_{2.5}$ enhancement, but did not always have an impact on the air pollution of the following day. The
392 pollution levels on the following day depended more on the strength of the cold front, local pollution
393 conditions, the structure of ABL and regional transportation. Further quantification is needed to
394 determine the relationship between the T-NPES events and the pollution levels on the following day.
395 Based on these mentioned above, we suggested that the T-NPES events were a common phenomenon in
396 winter in plain areas such as the NCP and the YRD. A conceptual model was thus developed and shown
397 in Figure 6, there were the transportation of aerosol by the horizontal winds above 1,000 m and the
398 updrafts dominated before night, which was conducive to the formation and suspension of the aerosol
399 layer. Then, as the southeasterly movement of the high-pressure system and the passage of the cold front
400 at about the time of midnight, the wind direction began to turn to north/northwest, causing the aerosol
401 diluted. Finally, the downdrafts dominated in the ABL and the LLJ might enhance the turbulent. Under
402 the influence of subsidence behind the cold front and turbulence, the depth of the aerosol layer suspended
403 above 1,000 m began to decrease and the pollutants gradually transported and diffused downwards into
404 the lower layer of the ABL, enhancing the concentration of surface $PM_{2.5}$.



405

406 **Figure 6.** Conceptual scheme of the T-NPES events

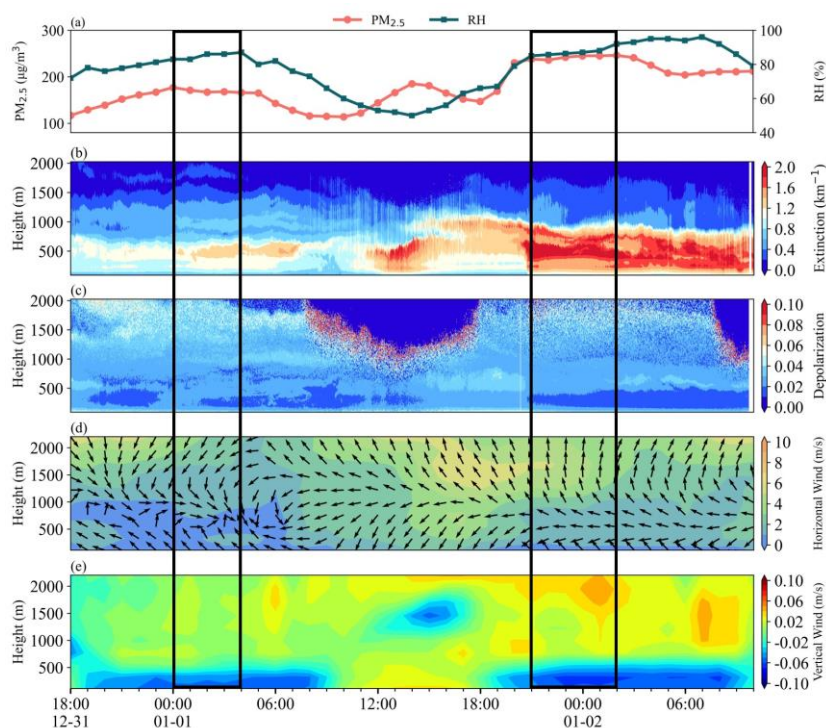
407 3.4 No T-NPES event occurred in Basin areas

408 We further checked the fix-point measurement in Xi'an and Chengdu, two cities with typical basin
409 topography. The results indicated that there were essentially no T-NPES events in either city, suggesting



410 the conceptual did not work. Figure 7(a) indicated that the concentration of surface $PM_{2.5}$ had no
411 enhancement during the night from 23:00 on 31 December to 4:00 on 1 January, and from 22:00 on 1
412 January to 3:00 on 2 January in Xi'an. $PM_{2.5}$ remained at a high concentration, while the extinction
413 coefficient did not show the subsidence process, suggesting that the T-NPES events were not common
414 here.

415 Taking the night of 31 December as an example, from 18:00 on 31 December to 4:00 on 1 January, the
416 concentration of surface $PM_{2.5}$ increased before 23:00 and then stabilized at high values, while the
417 extinction coefficient remained a high level with about $1.0\text{-}1.2\text{ km}^{-1}$ near 500 m. As shown in Figure 7(d),
418 from 18:00, 31 December to 6:00, 1 January, a light wind layer appeared below 1,000 m, with $\sim 1\text{ m/s}$.
419 Such a static and stable condition was conducive to the accumulation of locally generated particulate
420 matter near the ground, causing the concentration of $PM_{2.5}$ to enhance between 18:00 and 23:00 on 31
421 December and the formation and maintenance of the aerosol layer at about 500 m. Noteworthy, the wind
422 direction at low layer was southeaster, while it was the opposite northwester at about 1,000 m, which
423 was the typical characteristic of mountain-valley breeze circulation. The dominance of downdrafts below
424 500 m suggested that Xi'an was in the upper area of the nocturnal mountain-valley breeze circulation.
425 The mountain-valley breeze circulation could only be observed when the background WS was relatively
426 weak, which further indicated a stable structure of the ABL. The example on 1 January was similar to
427 the above one, with the extinction coefficient reaching 2 km^{-1} and depolarization ratio decreasing after
428 21:00 due to the hygroscopic growth of aerosol by the rise in relative humidity.



429

430 **Figure 7.** (a) Surface $PM_{2.5}$ concentration and relative humidity, (b) Extinction coefficient, (c) Depolarization ratio,
 431 (d) Horizontal wind, and (e) Vertical wind, during the observation in Xi'an from 18:00, 31 December to 10:00, 2
 432 January. The two black boxes were the time period to be studied.

433 Due to the topography of the basin in Xi'an, the mountain-valley breeze circulation, or the horizontal
 434 winds with lower WS always dominated in the ABL, which was not conducive to the transport and
 435 dispersion of particulate matter. The stable structure of the ABL resulted in the particulate matter
 436 accumulated in the low layer, which was the main feature of the nocturnal particulate matter
 437 distribution in Xi'an.

438 Figure 8 showed that the concentration of surface $PM_{2.5}$ also had no significant enhancement but
 439 remained a high value over nighttime in Chengdu. The distribution of the extinction coefficient in the
 440 two black boxes presented double-layer structure, one layer near 250 m and another layer suspended at
 441 about 500 m. Meanwhile, the wind field exhibited typical mountain-valley breeze circulation, as shown
 442 in the two black boxes in Figure 8(d), which presented westerly wind near 250 m and southeasterly wind
 443 above 500 m. The variation wind direction due to the mountain-valley breeze circulation at different
 444 layer might be responsible for the double-layer of particulate matter. Figure S13 illustrated the backward



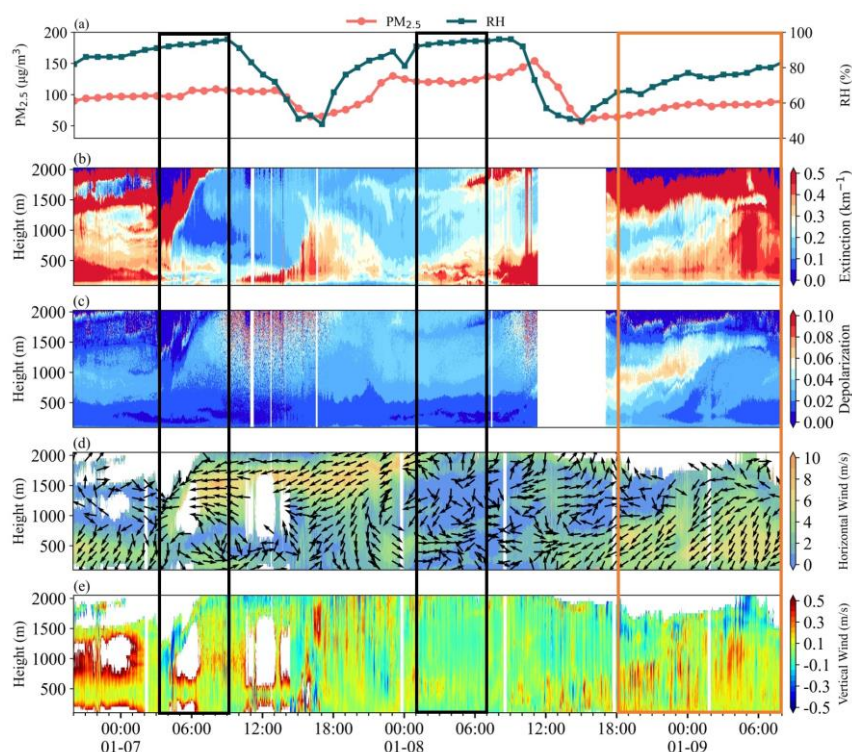
445 trajectories when the double-layer appeared. The layer of particulate matter at about 100 m might have
446 originated from the southwest area of Chengdu, whereas the layer of particulate matter at 500 m and
447 1,000 m might have originated from the northeast area of Chengdu. The different sources of particulate
448 matter were consistent with the mountain-valley breeze circulation in Chengdu, further demonstrating
449 the dominance of mountain-valley breeze in the static and stable ABL at night.

450 The orange box in Figure 8 indicated that the distribution of particulate matter in the ABL of Chengdu
451 under the dominance of northeasterly winds with high WS. Both extinction coefficient and the
452 depolarization ratio showed a stratified structure, with the extinction coefficient initially higher below
453 750 m and lower above 750 m, whereas the depolarization ratio exhibited the opposite trend. The main
454 cause of this phenomenon was that the different sources of particulate matter in the two layers. Under
455 the influence of the dominant updrafts, local emissions with high depolarization ratio were transported
456 upwards, while the lower layer was occupied by particulate matter with lower depolarization ratio
457 transported by the northeasterly wind. As the continuous transport of the northeasterly wind, the entire
458 ABL was occupied by transported particulate matter with a high extinction coefficient and a low
459 depolarization ratio.

460 Due to the short time during the fixed-point observation period, it is difficult to make a universal
461 conclusion that no T-NEPS occurs in basin regions. Therefore, we further checked the surface and model
462 simulation data of the two basin cities for three months in winter 2018. We found that, unlike the plain
463 area, the T-NEPS events were almost never observed in the basin regions. It confirmed that the
464 conceptual model was indeed not applicable in the basin area. This was mainly attributed to the fact that
465 the movement of the weather system was blocked by the mountains surrounding the basin. Therefore,
466 the movement of the high-pressure system and the passage of the cold front had a weak impact on the
467 basin region. Without the downdrafts and the shift in wind direction associated with the movement of
468 the high-pressure system and the passage of the cold front, the structure of the ABL between Xi'an and
469 Chengdu was relatively stable, making it difficult for particulate matter to be transported and diffused,
470 and thus accumulate in the ABL at night. During the three months, we found that the wind field in Xi'an
471 was dominated by the light winds, while in Chengdu there were two states: one is dominated by light
472 winds and the other by strong northeasterly wind. Fortunately, our fixed-point observations had captured
473 these typical processes indeed. In addition, considering the wind fields in basin cities were mainly
474 dominated by light winds, which was the main characteristic in basin area (Bei et al., 2016; Shu et al.,
475 2021) and was similar to the wind fields below 1,500 m in Taiyuan and Linfen of the Type 4. Therefore,



476 we suggested that the Loess Plateau cities might serve as a crucial transitional zone between the plains
477 and the basin as introduced in Section 3.3. In summary, the conceptual model of T-NPES events was
478 applicable to the plain areas which were more influenced by the movement of weather system in winter,
479 such as the NCP and YRD, but not to the basin areas.



480

481 **Figure 8.** (a) Surface $PM_{2.5}$ concentration and relative humidity, (b) Extinction coefficient, (c) Depolarization ratio,
482 (d) Horizontal wind, and (e) Vertical wind, during the observation in Chengdu from 20:00, 7 January to 8:00, 10
483 January. The two black boxes were the time period of the double-layer structure, the orange box was the time period
484 to be studied.

485 4 Conclusions and outlook

486 In this study, we reveal that the T-NPES is a relatively common and important pathway that causes $PM_{2.5}$
487 pollution in the surface layer in the plain areas in winter China. The fixed-point observations in
488 Changzhou and Wangdu demonstrated that the T-NPES was associated with the subsidence of particulate
489 matter in the upper layer due to the movement of high-pressure and the passage of the cold front. Model



490 simulations further confirmed the ubiquity of T-NPES events in plain areas, despite these event types
491 varied case by case. However, the observations in Xi'an and Chengdu indicated that the event was less
492 occurred in the basin areas, as the impact of weather system was weakened by the obstruction of
493 mountains surrounding the basin. In further studies, more multi-lidar measurement should be conducted
494 in other cities in the plains and basin areas to look insight to the detailed mechanism of T-NPES events.
495 In addition, more works are urgently needed to uncover the vertical profiles of chemical components of
496 the particulate matter, since it may also be affected by the coupling of physical and chemical processes.

497 **Code/Data availability.** The datasets used in this study are available at:
498 <https://doi.org/10.5281/zenodo.8368944> (Wang et al., 2023).

499 **Author contributions.** H.C.W. and S.J.F designed the study. Y.M.W. and H.C.W. analysed the data,
500 H.L.W. and X.L. provided the GEOS-Chem model simulation results, Y.M.W. and H.C.W. wrote the
501 paper with input from all coauthors.

502 **Competing interests.** The authors declare that they have no conflicts of interest.

503 **Acknowledgments.** The authors gratefully acknowledge the NOAA Air Resources Laboratory (ARL)
504 for the provision of the HYSPLIT transport and dispersion model used in this study.

505 **Financial support.** This research has been supported by the Guangdong Major Project of Basic and
506 Applied Basic Research (grant no. 2020B0301030004), the Guangdong science and technology plan
507 project (grant no. 2019B121201002), and the National Natural Science Foundation of China (grant no.
508 42175111).

509 **References**

510 An, Z.S., Huang, R.J., Zhang, R.Y., Tie, X.X., Li, G.H., Cao, J.J., Zhou, W.J., Shi, Z.G., Han, Y.M., Gu,
511 Z.L., Ji, Y.M.: Severe haze in northern China: A synergy of anthropogenic emissions and
512 atmospheric processes. P. Natl. Acad. Sci. USA. 116, 8657-8666.
513 <http://doi.org/10.1073/pnas.1900125116>, 2019



- 514 Bei, N.F., Xiao, B., Meng, N., Feng, T.: Critical role of meteorological conditions in a persistent haze
515 episode in the Guanzhong basin, China. *Sci. Total Environ.*, 550, 273-284.
516 <http://doi.org/10.1016/j.scitotenv.2015.12.159>, 2016
- 517 Bey, I., Jacob, D.J., Yantosca, R.M., Logan, J.A., Field, B.D., Fiore, A.M., Li, Q.B., Liu, H.G.Y.,
518 Mickley, L.J., Schultz, M.G.: Global modeling of tropospheric chemistry with assimilated
519 meteorology: Model description and evaluation. *J. Geophys. Res.: Atmos.*, 106, 23073-23095.
520 <http://doi.org/10.1029/2001JD000807>, 2001
- 521 Bian, H.S., Prather, M.J.: Fast-J2: Accurate simulation of stratospheric photolysis in global chemical
522 models. *J. Atmos. Chem.*, 41, 281-296. <http://doi.org/10.1023/A:1014980619462>, 2002
- 523 Cai, W.J., Li, K., Liao, H., Wang, H.J., Wu, L.X.: Weather conditions conducive to Beijing severe haze
524 more frequent under climate change. *Nat. Clim. Change.* 7, 257-+.
525 <http://doi.org/10.1038/NCLIMATE3249>, 2017
- 526 Callahan, C.W., Schnell, J.L., Horton, D.E.: Multi-Index Attribution of Extreme Winter Air Quality in
527 Beijing, China. *J. Geophys. Res.: Atmos.*, 124, 4567-4583.
528 <http://doi.org/10.1029/2018JD029738>, 2019
- 529 Carlson, M.A., Stull, R.B.: Subsidence in the nocturnal boundary layer. *J. Clim. Appl. Meteorol.*, 25,
530 1088-1099. [http://doi.org/10.1175/1520-0450\(1986\)025<1088:sitnbl>2.0.co;2](http://doi.org/10.1175/1520-0450(1986)025<1088:sitnbl>2.0.co;2), 1986
- 531 Chen, X.R., Wang, H.C., Lu, K.D., Li, C.M., Zhai, T.Y., Tan, Z.F., Ma, X.F., Yang, X.P., Liu, Y.H.,
532 Chen, S.Y., Dong, H.B., Li, X., Wu, Z.J., Hu, M., Zeng, L.M., Zhang, Y.H.: Field Determination
533 of Nitrate Formation Pathway in Winter Beijing. *Environ. Sci. Technol.*, 54, 9243-9253.
534 <http://doi.org/10.1021/acs.est.0c00972>, 2020
- 535 De Marco, A., Proietti, C., Anav, A., Ciancarella, L., D'Elia, I., Fares, S., Fornasier, M.F., Fusaro, L.,
536 Gualtieri, M., Manes, F., Marchetto, A., Mircea, M., Paoletti, E., Piersanti, A., Rogora, M.,
537 Salvati, L., Salvatori, E., Screpanti, A., Vialetto, G., Vitale, M., Leonardi, C.: Impacts of air
538 pollution on human and ecosystem health, and implications for the National Emission Ceilings
539 Directive: Insights from Italy. *Environ. Int.*, 125, 320-333.
540 <http://doi.org/10.1016/j.envint.2019.01.064>, 2019
- 541 Ding, A.J., Fu, C.B., Yang, X.Q., Sun, J.N., Petaja, T., Kerminen, V.M., Wang, T., Xie, Y., Herrmann,
542 E., Zheng, L.F., Nie, W., Liu, Q., Wei, X.L., Kulmala, M.: Intense atmospheric pollution
543 modifies weather: a case of mixed biomass burning with fossil fuel combustion pollution in



- 544 eastern China. *Atmos. Chem. Phys.*, 13, 10545-10554. [http://doi.org/10.5194/acp-13-10545-](http://doi.org/10.5194/acp-13-10545-2013)
545 [2013](http://doi.org/10.5194/acp-13-10545-2013), 2013
- 546 Ding, A.J., Huang, X., Nie, W., Chi, X.G., Xu, Z., Zheng, L.F., Xu, Z.N., Xie, Y.N., Qi, X.M., Shen,
547 Y.C., Sun, P., Wang, J.P., Wang, L., Sun, J.N., Yang, X.Q., Qin, W., Zhang, X.Z., Cheng, W.,
548 Liu, W.J., Pan, L.B., Fu, C.B.: Significant reduction of PM_{2.5} in eastern China due to regional-
549 scale emission control: evidence from SORPES in 2011-2018. *Atmos. Chem. Phys.*, 19, 11791-
550 11801. <http://doi.org/10.5194/acp-19-11791-2019>, 2019
- 551 Dong, Z.P., Li, Z.Q., Yu, X., Cribb, M., Li, X.M., Dai, J.: Opposite long-term trends in aerosols between
552 low and high altitudes: a testimony to the aerosol-PBL feedback. *Atmos. Chem. Phys.*, 17, 7997-
553 8009. <http://doi.org/10.5194/acp-17-7997-2017>, 2017
- 554 Dubey, R., Patra, A.K., Joshi, J., Blankenberg, D., Nazneen. Evaluation of vertical and horizontal
555 distribution of particulate matter near an urban roadway using an unmanned aerial vehicle. *Sci.*
556 *Total Environ.*, 836. <http://doi.org/10.1016/j.scitotenv.2022.155600>, 2022
- 557 Fast, J.D., Bell, D.M., Kulkarni, G., Liu, J.M., Mei, F., Saliba, G., Shilling, J.E., Suski, K., Tomlinson,
558 J., Wang, J., Zaveri, R., Zelenyuk, A.: Using aircraft measurements to characterize subgrid-
559 scale variability of aerosol properties near the Atmospheric Radiation Measurement Southern
560 Great Plains site. *Atmos. Chem. Phys.*, 22, 11217-11238. [http://doi.org/10.5194/acp-22-11217-](http://doi.org/10.5194/acp-22-11217-2022)
561 [2022](http://doi.org/10.5194/acp-22-11217-2022), 2022
- 562 Gao, M., Carmichael, G.R., Wang, Y., Saide, P.E., Yu, M., Xin, J., Liu, Z., Wang, Z.: Modeling study
563 of the 2010 regional haze event in the North China Plain. *Atmos. Chem. Phys.*, 16, 1673-1691.
564 <http://doi.org/10.5194/acp-16-1673-2016>, 2016
- 565 Gao, M., Liu, Z.R., Zheng, B., Ji, D.S., Sherman, P., Song, S.J., Xin, J.Y., Liu, C., Wang, Y.S., Zhang,
566 Q., Xing, J., Jiang, J.K., Wang, Z.F., Carmichael, G.R., McElroy, M.B.: China's emission
567 control strategies have suppressed unfavorable influences of climate on wintertime PM_{2.5}
568 concentrations in Beijing since 2002. *Atmos. Chem. Phys.*, 20, 1497-1505.
569 <http://doi.org/10.5194/acp-20-1497-2020>, 2020
- 570 Gao, M., Saide, P.E., Xin, J.Y., Wang, Y.S., Liu, Z.R., Wang, Y.X., Wang, Z.F., Pagowski, M.,
571 Guttikunda, S.K., Carmichael, G.R.: Estimates of Health Impacts and Radiative Forcing in
572 Winter Haze in Eastern China through Constraints of Surface PM_{2.5} Predictions. *Environ. Sci.*
573 *Technol.*, 51, 2178-2185. <http://doi.org/10.1021/acs.est.6b03745>, 2017



- 574 Gelaro, R., McCarty, W., Suarez, M.J., Todling, R., Molod, A., Takacs, L., Randles, C.A., Darmenov,
575 A., Bosilovich, M.G., Reichle, R., Wargan, K., Coy, L., Cullather, R., Draper, C., Akella, S.,
576 Buchard, V., Conaty, A., da Silva, A.M., Gu, W., Kim, G.K., Koster, R., Lucchesi, R., Merkova,
577 D., Nielsen, J.E., Partyka, G., Pawson, S., Putman, W., Rienecker, M., Schubert, S.D.,
578 Sienkiewicz, M., Zhao, B.: The Modern-Era Retrospective Analysis for Research and
579 Applications, Version 2 (MERRA-2). *J. Clim.*, 30, 5419-5454. [http://doi.org/10.1175/JCLI-D-](http://doi.org/10.1175/JCLI-D-16-0758.1)
580 [16-0758.1](http://doi.org/10.1175/JCLI-D-16-0758.1), 2017
- 581 Geng, G.N., Xiao, Q.Y., Liu, S.G., Liu, X.D., Cheng, J., Zheng, Y.X., Xue, T., Tong, D., Zheng, B.,
582 Peng, Y.R., Huang, X.M., He, K.B., Zhang, Q.: Tracking Air Pollution in China: Near Real-
583 Time PM_{2.5} Retrievals from Multisource Data Fusion. *Environ. Sci. Technol.*, 55, 12106-12115.
584 <http://doi.org/10.1021/acs.est.1c01863>, 2021a
- 585 Geng, G.N., Zheng, Y.X., Zhang, Q., Xue, T., Zhao, H.Y., Tong, D., Zheng, B., Li, M., Liu, F., Hong,
586 C.P., He, K.B., Davis, S.J.: Drivers of PM_{2.5} air pollution deaths in China 2002-2017. *Nat.*
587 *Geosci.*, 14, 645-+. <http://doi.org/10.1038/s41561-021-00792-3>, 2021b
- 588 Gramsch, E., Caceres, D., Oyola, P., Reyes, E., Vasquez, Y., Rubio, M.A., Sanchez, G.: Influence of
589 surface and subsidence thermal inversion on PM_{2.5} and black carbon concentration. *Atmos.*
590 *Environ.*, 98, 290-298. <http://doi.org/10.1016/j.atmosenv.2014.08.066>, 2014
- 591 Guo, S., Hu, M., Zamora, M.L., Peng, J.F., Shang, D.J., Zheng, J., Du, Z.F., Wu, Z., Shao, M., Zeng,
592 L.M., Molina, M.J., Zhang, R.Y.: Elucidating severe urban haze formation in China. *P. Natl.*
593 *Acad. Sci. USA.* 111, 17373-17378. <http://doi.org/10.1073/pnas.1419604111>, 2014
- 594 Hao, X., Li, J.D., Wang, H.J., Liao, H., Yin, Z.C., Hu, J.L., Wei, Y., Dang, R.J.: Long-term health impact
595 of PM_{2.5} under whole-year COVID-19 lockdown. *Environ. Pollut.*, 290.
596 <http://doi.org/10.1016/j.envpol.2021.118118>, 2021
- 597 He, C., Lu, X., Wang, H.L., Wang, H.C., Li, Y., He, G.W., He, Y.P., Wang, Y.R., Zhang, Y.L., Liu,
598 Y.M., Fan, Q., Fan, S.J.: The unexpected high frequency of nocturnal surface ozone
599 enhancement events over China: characteristics and mechanisms. *Atmos. Chem. Phys.*, 22,
600 15243-15261. <http://doi.org/10.5194/acp-22-15243-2022>, 2022
- 601 He, Y.P., Xu, X.Q., Gu, Z.L., Chen, X.H., Li, Y.M., Fan, S.J.: Vertical distribution characteristics of
602 aerosol particles over the Guanzhong Plain. *Atmos. Environ.*, 255.
603 <http://doi.org/10.1016/j.atmosenv.2021.118444>, 2021



- 604 Hu, X.-M., Klein, P.M., Xue, M., Zhang, F., Doughty, D.C., Forkel, R., Joseph, E., Fuentes, J.D.: Impact
605 of the vertical mixing induced by low-level jets on boundary layer ozone concentration. *Atmos.*
606 *Environ.*, 70, 123-130. <http://doi.org/10.1016/j.atmosenv.2012.12.046>, 2013
- 607 Huang, R.J., Zhang, Y.L., Bozzetti, C., Ho, K.F., Cao, J.J., Han, Y.M., Daellenbach, K.R., Slowik, J.G.,
608 Platt, S.M., Canonaco, F., Zotter, P., Wolf, R., Pieber, S.M., Bruns, E.A., Crippa, M., Ciarelli,
609 G., Piazzalunga, A., Schwikowski, M., Abbaszade, G., Schnelle-Kreis, J., Zimmermann, R., An,
610 Z.S., Szidat, S., Baltensperger, U., El Haddad, I., Prevot, A.S.H.: High secondary aerosol
611 contribution to particulate pollution during haze events in China. *Nature*. 514, 218-222.
612 <http://doi.org/10.1038/nature13774>, 2014
- 613 Huang, X., Ding, A.J., Wang, Z.L., Ding, K., Gao, J., Chai, F.H., Fu, C.B.: Amplified transboundary
614 transport of haze by aerosol-boundary layer interaction in China. *Nat. Geosci.*, 13, 428-+.
615 <http://doi.org/10.1038/s41561-020-0583-4>, 2020
- 616 Huang, X., Wang, Z.L., Ding, A.J.: Impact of Aerosol-PBL Interaction on Haze Pollution: Multiyear
617 Observational Evidences in North China. *Geophys. Res. Lett.*, 45, 8596-8603.
618 <http://doi.org/10.1029/2018GL079239>, 2018
- 619 Kang, H.Q., Zhu, B., Gao, J.H., He, Y., Wang, H.L., Su, J.F., Pan, C., Zhu, T., Yu, B.: Potential impacts
620 of cold frontal passage on air quality over the Yangtze River Delta, China. *Atmos. Chem. Phys.*,
621 19, 3673-3685. <http://doi.org/10.5194/acp-19-3673-2019>, 2019
- 622 Kang, H.Q., Zhu, B., Liu, X.H., Shi, S.S., Hou, X.W., Lu, W., Yan, S.Q., Pan, C., Chen, Y.: Three-
623 Dimensional Distribution of PM_{2.5} over the Yangtze River Delta as Cold Fronts Moving
624 Through. *J. Geophys. Res.: Atmos.*, 126. <http://doi.org/10.1029/2020JD034035>, 2021
- 625 Kraus, H., Malcher, J., Schaller, E.: A nocturnal low level jet during PUKK. *Bound.-Layer Meteorol.*
626 (Netherlands). 31, 187-195. <http://doi.org/10.1007/bf00121177>, 1985
- 627 Largeron, Y., Staquet, C.: Persistent inversion dynamics and wintertime PM₁₀ air pollution in Alpine
628 valleys. *Atmos. Environ.*, 135, 92-108. <http://doi.org/10.1016/j.atmosenv.2016.03.045>, 2016
- 629 Li, H.Y., Cheng, J., Zhang, Q., Zheng, B., Zhang, Y.X., Zheng, G.J., He, K.B.: Rapid transition in winter
630 aerosol composition in Beijing from 2014 to 2017: response to clean air actions. *Atmos. Chem.*
631 *Phys.*, 19, 11485-11499. <http://doi.org/10.5194/acp-19-11485-2019>, 2019a
- 632 Li, L., Lu, C., Chan, P.W., Lan, Z.J., Zhang, W.H., Yang, H.L., Wang, H.C.: Impact of the COVID-19
633 on the vertical distributions of major pollutants from a tower in the Pearl River Delta. *Atmos.*
634 *Environ.*, 276. <http://doi.org/10.1016/j.atmosenv.2022.119068>, 2022



- 635 Li, Z.Q., Guo, J.P., Ding, A.J., Liao, H., Liu, J.J., Sun, Y.L., Wang, T.J., Xue, H.W., Zhang, H.S., Zhu,
636 B.: Aerosol and boundary-layer interactions and impact on air quality. *Natl. Sci. Rev.*, 4, 810-
637 833. <http://doi.org/10.1093/nsr/nwx117>, 2017
- 638 Li, Z.Q., Wang, Y., Guo, J.P., Zhao, C.F., Cribb, M., Dong, X.Q., Fan, J.W., Gong, D.Y., Huang, J.P.,
639 Jiang, M.J., Jiang, Y.Q., Lee, S.S., Li, H., Li, J.M., Liu, J.J., Qian, Y., Rosenfeld, D., Shan, S.Y.,
640 Sun, Y.L., Wang, H.J., Xin, J.Y., Yan, X., Yang, X., Yang, X.Q., Zhang, F., Zheng, Y.T.: East
641 Asian Study of Tropospheric Aerosols and their Impact on Regional Clouds, Precipitation, and
642 Climate (EAST-AIR(CPC)). *J. Geophys. Res.: Atmos.*, 124, 13026-13054.
643 <http://doi.org/10.1029/2019JD030758>, 2019b
- 644 Lin, J.T., McElroy, M.B.: Impacts of boundary layer mixing on pollutant vertical profiles in the lower
645 troposphere: Implications to satellite remote sensing. *Atmos. Environ.*, 44, 1726-1739.
646 <http://doi.org/10.1016/j.atmosenv.2010.02.009>, 2010
- 647 Lu, K.D., Fuchs, H., Hofzumahaus, A., Tan, Z.F., Wang, H.C., Zhang, L., Schmitt, S.H., Rohrer, F.,
648 Bohn, B., Broch, S., Dong, H.B., Gkatzelis, G.I., Hohaus, T., Holland, F., Li, X., Liu, Y., Liu,
649 Y.H., Ma, X.F., Novelli, A., Schlag, P., Shao, M., Wu, Y.S., Wu, Z.J., Zeng, L.M., Hu, M.,
650 Kiendler-Scharr, A., Wahner, A., Zhang, Y.H.: Fast Photochemistry in Wintertime Haze:
651 Consequences for Pollution Mitigation Strategies. *Environ. Sci. Technol.*, 53, 10676-10684.
652 <http://doi.org/10.1021/acs.est.9b02422>, 2019
- 653 Lv, L., Xiang, Y., Zhang, T., Chai, W., Liu, W.: Comprehensive study of regional haze in the North
654 China Plain with synergistic measurement from multiple mobile vehicle-based lidars and a lidar
655 network. *Sci. Total Environ.*, 721. <http://doi.org/10.1016/j.scitotenv.2020.137773>, 2020
- 656 Mao, J., Fan, S., Jacob, D.J., Travis, K.R.: Radical loss in the atmosphere from Cu-Fe redox coupling in
657 aerosols. *Atmos. Chem. Phys.*, 13, 509-519. <http://doi.org/10.5194/acp-13-509-2013>, 2013
- 658 Munoz-Sabater, J., Dutra, E., Agusti-Panareda, A., Albergel, C., Arduini, G., Balsamo, G., Boussetta, S.,
659 Choulga, M., Harrigan, S., Hersbach, H., Martens, B., Miralles, D.G., Piles, M., Rodriguez-
660 Fernandez, N.J., Zsoter, E., Buontempo, C., Thepaut, J.N.: ERA5-Land: a state-of-the-art global
661 reanalysis dataset for land applications. *Earth Syst. Sci. Data.* 13, 4349-4383.
662 <http://doi.org/10.5194/essd-13-4349-2021>, 2021
- 663 O'Rourke, P.R., Smith, S.J., Mott, A., Ahsan, H., McDuffie, E.E., Crippa, M., Klimont, S., McDonald,
664 B., Z., W., Nicholson, M.B., Feng, L., Hoesly, R.M., 2021. CEDS v-2021-04-21 Emission Data
665 1975-2019 (Version Apr-21-2021).



- 666 Park, R.J., Jacob, D.J., Field, B.D., Yantosca, R.M., Chin, M.: Natural and transboundary pollution
667 influences on sulfate-nitrate-ammonium aerosols in the United States: Implications for policy.
668 J. Geophys. Res.: Atmos., 109. <http://doi.org/10.1029/2003JD004473>, 2004
- 669 Parrella, J.P., Jacob, D.J., Liang, Q., Zhang, Y., Mickley, L.J., Miller, B., Evans, M.J., Yang, X., Pyle,
670 J.A., Theys, N., Van Roozendaal, M.: Tropospheric bromine chemistry: implications for present
671 and pre-industrial ozone and mercury. Atmos. Chem. Phys., 12, 6723-6740.
672 <http://doi.org/10.5194/acp-12-6723-2012>, 2012
- 673 Peng, J.F., Hu, M., Shang, D.J., Wu, Z.J., Du, Z.F., Tan, T.Y., Wang, Y.N., Zhang, F., Zhang, R.Y.:
674 Explosive Secondary Aerosol Formation during Severe Haze in the North China Plain. Environ.
675 Sci. Technol., 55, 2189-2207. <http://doi.org/10.1021/acs.est.0c07204>, 2021
- 676 Qin, Y., Li, J.Y., Gong, K.J., Wu, Z.J., Chen, M.D., Qin, M.M., Huang, L., Hu, J.L.: Double high
677 pollution events in the Yangtze River Delta from 2015 to 2019: Characteristics, trends, and
678 meteorological situations. Sci. Total Environ., 792.
679 <http://doi.org/10.1016/j.scitotenv.2021.148349>, 2021
- 680 Ran, L., Deng, Z.Z., Wu, Y.F., Li, J.W., Bai, Z.X., Lu, Y., Zhuoga, D.Q., Bian, J.C.: Measurement report:
681 Vertical profiling of particle size distributions over Lhasa, Tibet - tethered balloon-based in situ
682 measurements and source apportionment. Atmos. Chem. Phys., 22, 6217-6229.
683 <http://doi.org/10.5194/acp-22-6217-2022>, 2022
- 684 Shi, C.N., Nduka, I.C., Yang, Y.J., Huang, Y., Yao, R.S., Zhang, H., He, B.F., Xie, C.B., Wang, Z.Z.,
685 Yim, S.H.L.: Characteristics and meteorological mechanisms of transboundary air pollution in
686 a persistent heavy PM_{2.5} pollution episode in Central-East China. Atmos. Environ., 223.
687 <http://doi.org/10.1016/j.atmosenv.2019.117239>, 2020
- 688 Shi, Y., Zeng, Q.C., Liu, L., Huo, J.T., Zhang, Z., Ding, W.C., Hu, F.: Observed Evidence That
689 Subsidence Process Stabilizes the Boundary Layer and Increases the Ground Concentration of
690 Secondary Pollutants. J. Geophys. Res.: Atmos., 127. <http://doi.org/10.1029/2021JD035244>,
691 2022
- 692 Shu, Z.Z., Liu, Y.B., Zhao, T.L., Xia, J.R., Wang, C.G., Cao, L., Wang, H.L., Zhang, L., Zheng, Y., Shen,
693 L.J., Luo, L., Li, Y.Q.: Elevated 3D structures of PM_{2.5} and impact of complex terrain-forcing
694 circulations on heavy haze pollution over Sichuan Basin, China. Atmos. Chem. Phys., 21, 9253-
695 9268. <http://doi.org/10.5194/acp-21-9253-2021>, 2021



- 696 Silver, B., Conibear, L., Reddington, C.L., Knote, C., Arnold, S.R., Spracklen, D.V.: Pollutant emission
697 reductions deliver decreased PM_{2.5}-caused mortality across China during 2015-2017. *Atmos.*
698 *Chem. Phys.*, 20, 11683-11695. <http://doi.org/10.5194/acp-20-11683-2020>, 2020
- 699 Song, R.F., Wang, D.S., Li, X.B., Li, B., Peng, Z.R., He, H.D.: Characterizing vertical distribution
700 patterns of PM_{2.5} in low troposphere of Shanghai city, China: Implications from the perspective
701 of unmanned aerial vehicle observations. *Atmos. Environ.*, 265.
702 <http://doi.org/10.1016/j.atmosenv.2021.118724>, 2021
- 703 Stein, A.F., Draxler, R.R., Rolph, G.D., Stunder, B.J.B., Cohen, M.D., Ngan, F.: NOAA'S HYSPLIT
704 ATMOSPHERIC TRANSPORT AND DISPERSION MODELING SYSTEM. *Bull. Am.*
705 *Meteorol. Soc.*, 96, 2059-2077. <http://doi.org/10.1175/BAMS-D-14-00110.1>, 2015
- 706 Wang, D.F., Huo, J.T., Duan, Y.S., Zhang, K., Ding, A.J., Fu, Q.Y., Luo, J.H., Fei, D.N., Xiu, G.L.,
707 Huang, K.: Vertical distribution and transport of air pollutants during a regional haze event in
708 eastern China: A tethered mega-balloon observation study. *Atmos. Environ.*, 246.
709 <http://doi.org/10.1016/j.atmosenv.2020.118039>, 2021
- 710 Wang, F., Li, Z.Q., Ren, X.R., Jiang, Q., He, H., Dickerson, R.R., Dong, X.B., Lv, F.: Vertical
711 distributions of aerosol optical properties during the spring 2016 ARIAs airborne campaign in
712 the North China Plain. *Atmos. Chem. Phys.*, 18, 8995-9010. [http://doi.org/10.5194/acp-18-](http://doi.org/10.5194/acp-18-8995-2018)
713 [8995-2018](http://doi.org/10.5194/acp-18-8995-2018), 2018
- 714 Wang, H.C., Lu, K.D., Chen, X.R., Zhu, Q.D., Chen, Q., Guo, S., Jiang, M.Q., Li, X., Shang, D.J., Tan,
715 Z.F., Wu, Y.S., Wu, Z.J., Zou, Q., Zheng, Y., Zeng, L.M., Zhu, T., Hu, M., Zhang, Y.H.: High
716 N₂O₅ Concentrations Observed in Urban Beijing: Implications of a Large Nitrate Formation
717 Pathway. *Environ. Sci. Technol. Lett.*, 4, 416-420. <http://doi.org/10.1021/acs.estlett.7b00341>,
718 2017
- 719 Wang, Y.H., Logan, J.A., Jacob, D.J.: Global simulation of tropospheric O₃-NO_x-hydrocarbon
720 chemistry. 2. Model evaluation and global ozone budget. *J. Geophys. Res. (USA)*. 103, 10727-
721 10755. <http://doi.org/10.1029/98jd00157>, 1998
- 722 Wang, Y.M., Wang, H.C., Fan, S.J.: Measurement report: Nocturnal subsidence behind the cold front
723 enhances surface particulate matter in the plain regions: observation from the mobile multi-lidar
724 system [Data set], <https://doi.org/10.5281/zenodo.8368944>, 2023.



- 725 Wesely, M.L.: Parameterization of surface resistances to gaseous dry deposition in regional-scale
726 numerical models. *Atmos. Environ.*, 23, 1293-1304. [http://doi.org/10.1016/0004-
727 6981\(89\)90153-4](http://doi.org/10.1016/0004-6981(89)90153-4), 1989
- 728 WHO. WHO Global Air Quality Guidelines: Particulate Matter (PM_{2.5} and PM₁₀), Ozone, Nitrogen
729 Dioxide, Sulfur Dioxide and Carbon Monoxide, World Health Organization (WHO), Geneva,
730 Switzerland., 2021
- 731 Xiao, Q.Y., Geng, G.N., Cheng, J., Liang, F.C., Li, R., Meng, X., Xue, T., Huang, X.M., Kan, H.D.,
732 Zhang, Q., He, K.B.: Evaluation of gap-filling approaches in satellite-based daily PM_{2.5}
733 prediction models. *Atmos. Environ.*, 244. <http://doi.org/10.1016/j.atmosenv.2020.117921>,
734 2021a
- 735 Xiao, Q.Y., Zheng, Y.X., Geng, G.N., Chen, C.H., Huang, X.M., Che, H.Z., Zhang, X.Y., He, K.B.,
736 Zhang, Q.: Separating emission and meteorological contributions to long-term PM_{2.5} trends over
737 eastern China during 2000-2018. *Atmos. Chem. Phys.*, 21, 9475-9496.
738 <http://doi.org/10.5194/acp-21-9475-2021>, 2021b
- 739 Xu, X.Q., Xie, J.L., Li, Y.M., Miao, S.J., Fan, S.J.: Measurement report: Vehicle-based multi-lidar
740 observational study of the effect of meteorological elements on the three-dimensional
741 distribution of particles in the western Guangdong-Hong Kong-Macao Greater Bay Area.
742 *Atmos. Chem. Phys.*, 22, 139-153. <http://doi.org/10.5194/acp-22-139-2022>, 2022
- 743 Xu, Z.N., Huang, X., Nie, W., Shen, Y.C., Zheng, L.F., Xie, Y.N., Wang, T.Y., Ding, K., Liu, L.X.,
744 Zhou, D.R., Qi, X.M., Ding, A.J.: Impact of Biomass Burning and Vertical Mixing of Residual-
745 Layer Aged Plumes on Ozone in the Yangtze River Delta, China: A Tethered-Balloon
746 Measurement and Modeling Study of a Multiday Ozone Episode. *J. Geophys. Res.: Atmos.*,
747 123, 11786-11803. <http://doi.org/10.1029/2018JD028994>, 2018
- 748 Yin, C.Q., Xu, J.M., Gao, W., Pan, L., Gu, Y.X., Fu, Q.Y., Yang, F.: Characteristics of fine particle
749 matter at the top of Shanghai Tower. *Atmos. Chem. Phys.*, 23, 1329-1343.
750 <http://doi.org/10.5194/acp-23-1329-2023>, 2023
- 751 Yue, X., Unger, N., Harper, K., Xia, X.G., Liao, H., Zhu, T., Xiao, J.F., Feng, Z.Z., Li, J.: Ozone and
752 haze pollution weakens net primary productivity in China. *Atmos. Chem. Phys.*, 17, 6073-6089.
753 <http://doi.org/10.5194/acp-17-6073-2017>, 2017
- 754 Zhang, G., Gao, Y., Cai, W.J., Leung, L.R., Wang, S.X., Zhao, B., Wang, M.H., Shan, H.Y., Yao, X.H.,
755 Gao, H.W.: Seesaw haze pollution in North China modulated by the sub-seasonal variability of



- 756 atmospheric circulation. *Atmos. Chem. Phys.*, 19, 565-576. [http://doi.org/10.5194/acp-19-565-](http://doi.org/10.5194/acp-19-565-2019)
757 [2019](http://doi.org/10.5194/acp-19-565-2019), 2019a
- 758 Zhang, L.M., Gong, S.L., Padro, J., Barrie, L.: A size-segregated particle dry deposition scheme for an
759 atmospheric aerosol module. *Atmos. Environ.*, 35, 549-560. [http://doi.org/10.1016/S1352-](http://doi.org/10.1016/S1352-2310(00)00326-5)
760 [2310\(00\)00326-5](http://doi.org/10.1016/S1352-2310(00)00326-5), 2001
- 761 Zhang, Q., Zheng, Y.X., Tong, D., Shao, M., Wang, S.X., Zhang, Y.H., Xu, X.D., Wang, J.N., He, H.,
762 Liu, W.Q., Ding, Y.H., Lei, Y., Li, J.H., Wang, Z.F., Zhang, X.Y., Wang, Y.S., Cheng, J., Liu,
763 Y., Shi, Q.R., Yan, L., Geng, G.N., Hong, C.P., Li, M., Liu, F., Zheng, B., Cao, J.J., Ding, A.J.,
764 Gao, J., Fu, Q.Y., Huo, J.T., Liu, B.X., Liu, Z.R., Yang, F.M., He, K.B., Hao, J.M.: Drivers of
765 improved PM_{2.5} air quality in China from 2013 to 2017. *P. Natl. Acad. Sci. USA.* 116, 24463-
766 24469. <http://doi.org/10.1073/pnas.1907956116>, 2019b
- 767 Zhang, R.Y., Wang, G.H., Guo, S., Zarnora, M.L., Ying, Q., Lin, Y., Wang, W.G., Hu, M., Wang, Y.:
768 Formation of Urban Fine Particulate Matter. *Chem. Rev.*, 115, 3803-3855.
769 <http://doi.org/10.1021/acs.chemrev.5b00067>, 2015
- 770 Zhang, W.H., Li, W.S., An, X.D., Zhao, Y.H., Sheng, L.F., Hai, S.F., Li, X.D., Wang, F., Zi, Z.F., Chu,
771 M.: Numerical study of the amplification effects of cold-front passage on air pollution over the
772 North China Plain. *Sci. Total Environ.*, 833. <http://doi.org/10.1016/j.scitotenv.2022.155231>,
773 2022
- 774 Zhao, X.J., Zhao, P.S., Xu, J., Meng, W., Pu, W.W., Dong, F., He, D., Shi, Q.F.: Analysis of a winter
775 regional haze event and its formation mechanism in the North China Plain. *Atmos. Chem. Phys.*,
776 13, 5685-5696. <http://doi.org/10.5194/acp-13-5685-2013>, 2013
- 777 Zhao, X.X., Zhao, X.J., Liu, P.F., Chen, D., Zhang, C.L., Xue, C.Y., Liu, J.F., Xu, J., Mu, Y.J.: Transport
778 Pathways of Nitrate Formed from Nocturnal N₂O₅ Hydrolysis Aloft to the Ground Level in
779 Winter North China Plain. *Environ. Sci. Technol.* <http://doi.org/10.1021/acs.est.3c00086>, 2023
- 780 Zheng, B., Tong, D., Li, M., Liu, F., Hong, C.P., Geng, G.N., Li, H.Y., Li, X., Peng, L.Q., Qi, J., Yan,
781 L., Zhang, Y.X., Zhao, H.Y., Zheng, Y.X., He, K.B., Zhang, Q.: Trends in China's
782 anthropogenic emissions since 2010 as the consequence of clean air actions. *Atmos. Chem.*
783 *Phys.*, 18, 14095-14111. <http://doi.org/10.5194/acp-18-14095-2018>, 2018
- 784 Zhou, X., Huang, X., Sun, P., Chi, X., Ren, C., Lai, S., Wang, Z., Qi, X., Wang, J., Nie, W., Xu, Z., Huo,
785 J., Fu, Q., Ding, A.: Fast Secondary Aerosol Formation in Residual Layer and Its Impact on Air

<https://doi.org/10.5194/egusphere-2023-2178>

Preprint. Discussion started: 9 October 2023

© Author(s) 2023. CC BY 4.0 License.



786 Pollution Over Eastern China. J. Geophys. Res.: Atmos., 128, e2023JD038501.

787 <http://doi.org/https://doi.org/10.1029/2023JD038501>, 2023

788